JOURNAL OF PROPULSION AND POWER
Vol. 26, No. 5, September–October 2010

Nozzle-Geometry Effects on Upwind-Surface Properties of Turbulent Liquid Jets in Gaseous Crossflow

A. R. Osta* and K. A. Sallam†
Oklahoma State University, Stillwater, Oklahoma 74078

DOI: 10.2514/1.49737

An experimental study to investigate the effect of nozzle length-to-diameter ratio and the inlet curvature on the surface properties of turbulent liquid jets in gaseous crossflow was carried out. Straight nozzles with length/diameter ratios of 10, 20, and 40 were used to generate turbulent liquid jets in gaseous crossflow. The radius of curvature of the nozzles used was 0.6, 1.2, and 2.4. The present study was limited to small Ohnesorge number liquid jets ($Oh < 0.01$) injected in crossflow within the shear breakup regime ($We_G > 110$). The diagnostics consisted of double-pulsed holographic microscopy and shadowgraphy. The measurements included liquid-jet surface properties, breakup location of the liquid column as a whole, and the breakup-regime transitions. The measurements were interpreted and correlated using phenomenological analyses. It was observed that the injector passage length plays a role in determining the breakup length and influences the characteristics of the jet upwind surface.

Nomenclature

D	=	inner diameter of the nozzle
d_j	=	jet exit diameter
L	=	length of the nozzle passage
Oh	=	Ohnesorge number, $\mu_L/(\rho_L d_j \sigma)^{1/2}$
q	=	flow momentum ratio ($\rho_L v_j^2/\rho_G u_G^2$)
Re_G	=	cross-stream Reynolds number ($\rho_G u_G d_j/\mu_G$)
Re_{Ld}	=	liquid-jet Reynolds number ($\rho_L v_j d_j/\mu_L$)
t	=	time
u	=	cross-stream velocity (in the horizontal direction)
v	=	streamwise velocity (in the vertical direction)
We_G	=	crossflow Weber number ($\rho_G d_j u_G^2/\sigma$)
$We_{L\Lambda}$	=	jet Weber number ($\rho_L \Lambda v_j^2/\sigma$)
x	=	cross-stream distance (horizontal)
y	=	downstream distance (vertical)
μ	=	viscosity
Λ	=	turbulence integral length scale, $d_j/8$
λ	=	length scale corresponding to ligament and drop size during primary breakup
ρ_G	=	gas density
ρ_L	=	liquid density
σ	=	surface tension

Subscripts

b	=	end of the liquid-core property
G	=	gas property
j	=	jet exit property
L	=	liquid property
lig	=	ligament property
∞	=	freestream property

I. Introduction

THE breakup of liquid jets in crossflow (see Fig. 1) is specifically relevant to many propulsion applications such as in gas turbines and ramjet engines. The study of the effect of a plain orifice atomizer with a finite straight-passage length on the breakup of turbulent liquid jet injected by it in uniform crossflow was motivated by its relevant application to fuel injection systems in jet engines for which rapid fuel penetration, mixing with crossflow, and sustainment of combustion are desired. It is known that the disintegration of a cylindrical liquid jet in a quiescent atmosphere arises from the growth of perturbations initiated at or before the ejection nozzle. The disintegration process for turbulent liquid jets is brought about by the breakup of the ligaments, which have been generated by the jet surface instabilities into droplets. As pointed out by [1,2] the injector geometry influences the liquid-jet breakup, whereas the turbulence and cavitation within the nozzle are factors that can decisively cause the breakup of the liquid jet. The role played by the internal turbulence in the liquid jet can never be ruled out as a high degree of turbulence in a jet could initiate jet instability and be the driving mechanism in causing the jet to disintegrate earlier than it would due to the aerodynamic interplay alone. In most practical cases, however, one would expect that the instability initiated by the turbulence to get amplified by the aerodynamic forces acting on the jet and that the cumulative effect causes the jet to disintegrate. In practical injectors sharp-edged injector entry causes cavitation to be generated within the nozzle. The upwind-surface instabilities are most likely influenced by the turbulent shear stresses.

Early work on atomization of turbulent liquid jets was conducted by [3–8], among others. Later studies carried out by [9–14] have shown that the liquid-jet breakup in still air was significantly influenced by the geometry of the injector passage, which could be designed to control the fuel atomization quality. McCarthy and Molloy [9] explained the effects of injector geometry and internal flow conditions on the breakup of glycerol–water jets in still air and showed that for increasing L/D ratios, the roughness of the jet surface increased, which resulted in the jet breakup changing from the varicose type to the secondary atomization one, as shown in Fig. 2. Hiroyasu et al. [11–13] studied high-velocity jet breakup, as encountered in diesel engines, and observed that cavitation at the nozzle's entrance decreased the breakup length in general. This cavitation could be controlled by the jet velocity and the nozzle entry (shown in Fig. 3b), and for strong cavitation, the flow reattachment in the nozzle resulted in increasing breakup lengths. The results were less pronounced for high-pressure atmospheres (3 MPa), because the aerodynamic effects far outweighed the hydrodynamic instabilities. Wu et al. [15,16] showed that the boundary layer generated along the injector passage walls led to jet surface instabilities. Hiroyasu et al. [11,12] and Arai et al. [14], carried out similar tests for Reynolds numbers higher than 30,000 and observed that for L/D ratios up to 50, the breakup length increased with L/D, because the strong turbulence created by separation at the nozzle entrance was reduced

Presented as Paper 2009-1374 at the 47th AIAA Aerospace Sciences Meeting, Orlando, FL, 5–8 January 2009; received 5 March 2010; revision received 1 July 2010; accepted for publication 8 July 2010.

*Graduate Student, Mechanical and Aerospace Engineering; anu.osta@okstate.edu (Corresponding Author).

†Associate Professor, Mechanical and Aerospace Engineering; khaled.sallam@okstate.edu. Senior Member AIAA.

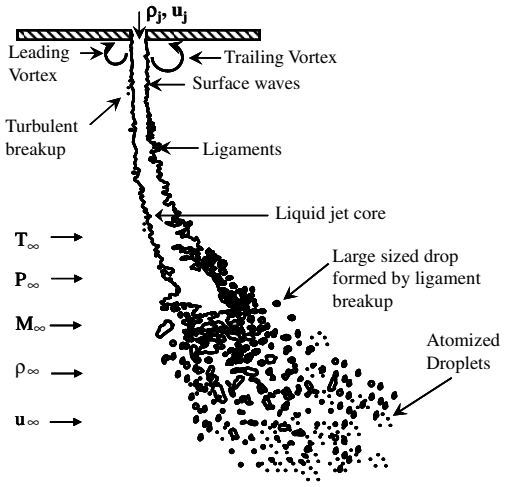

Fig. 1 Schematic of a turbulent liquid-jet breakup in uniform crossflow.

and the internal nozzle flow profile became fully developed [12]. In the spray region, however, the increase in the nozzle aspect ratio caused separation and cavitation, exhibiting hysteresis effects, resulting in changes in the nozzle's internal flow pattern and the corresponding jets having short breakup lengths. Other studies [8,12] suggested that the liquid turbulence has a great effect on jet stability, the onset of breakup, and spray quality after breakup.

Sterling and Sleicher [10] compared the results of breakup of capillary jets at high jet velocities from nozzles with $L/D = 0$, 49, and 96 (Fig. 3) and found the jet length to be in disagreement with the prevailing theories, due to overestimation of the aerodynamic

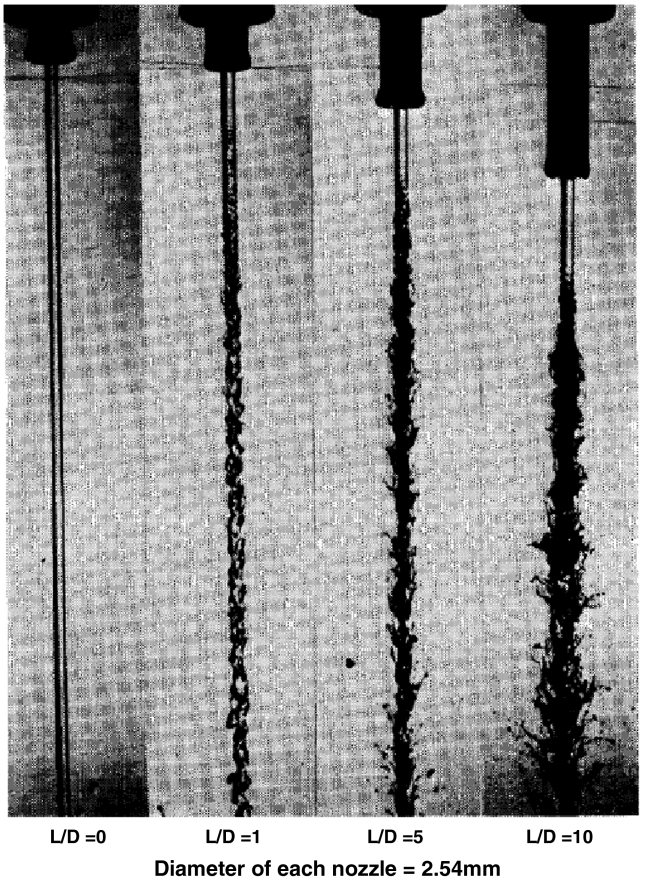

Fig. 2 Effect of nozzle L/D on the stability of glycerol–water jets. At the extreme left $L/D = 0$ and the breakup regime (not shown in the field of view) is varicose, and on the extreme right $L/D = 10$ and the breakup regime is secondary atomization (McCarthy and Molloy [9]).

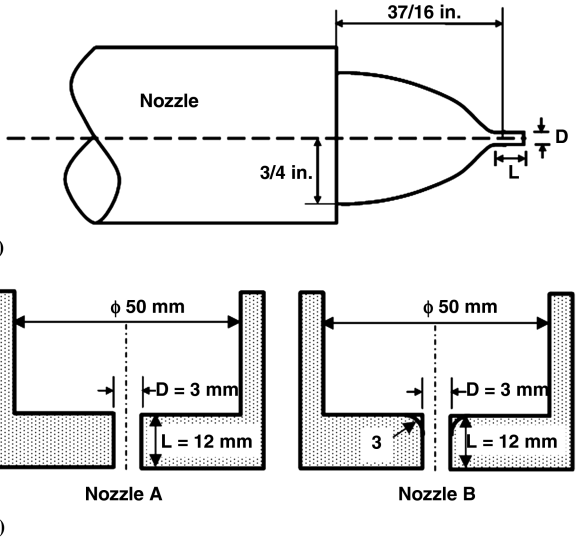

Fig. 3 Nozzle geometry used by a) Sterling and Sleicher [10] and b) Hiroyasu [13] (both A and B).

factors. They proposed a modification to Weber's theory considering the effect of ambient fluid viscosity on the normal stresses at the jet surface.

Breakup properties of turbulent liquid jets in crossflow for different fluids and conditions, including atomization of the liquid core, has been pursued by Wu et al. [17], Cavaliere et al. [18], Yoon [19], Zhang et al. [20], Bellofiore et al. [21], Birouk et al. [22], and Mashayek and Ashgriz [23]. Their respective nozzles are shown in Fig. 4a [17], Fig. 4b [22], and Fig. 4c [21]. A concern about their findings, however, is that the effect of L/D on the upwind-surface characteristics in the shear breakup regime is lacking. This is of interest because the jet upwind surface represents the strength of the turbulence in the jet. Since the upwind surface experiences the opposing aerodynamic force first, it influences the cycle of events that follow for a jet in crossflow.

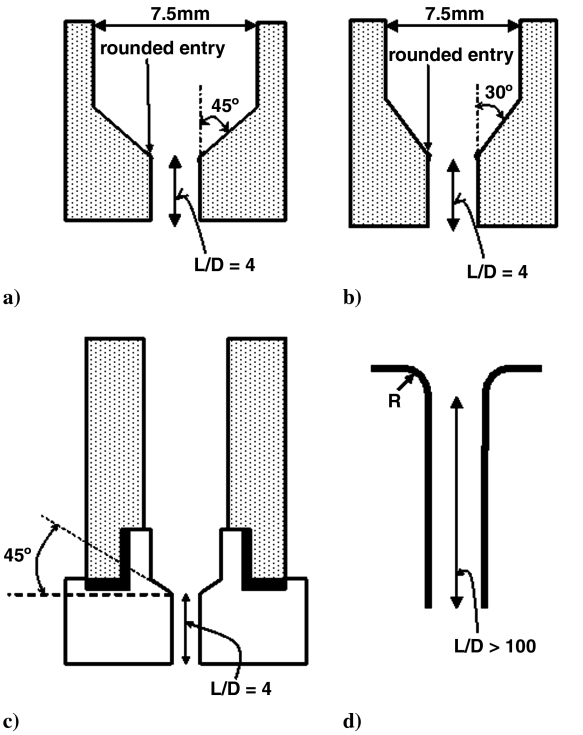

Fig. 4 Nozzle geometry of a) Wu et al. [17], b) Birouk et al. [22], c) Bellofiore et al. [21], and d) Lee et al. [24].

Lee et al. [24] carried out investigation on the breakup of fully turbulent liquid jets ($L/D > 100$, see Fig. 4d) in crossflow and compared their results to the breakup of nonturbulent liquid jet ($L/D = 0$) in crossflow [25] at conditions in which liquid viscosity had negligible effect (Ohnesorge numbers were less than 0.12). They observed that the formation of ligaments and drops on the downwind side was enhanced by the presence of crossflow, which was due to a reduction in the pressure along the sides of the liquid jet. The onset of turbulent primary breakup was accelerated because of this reduction in pressure and it always occurred at some distance from the jet exit, approaching the jet exit at large jet Weber numbers. The breakup times of the turbulent liquid jets were smaller than those for nonturbulent liquid jets [25]. A concern is that the behavior of liquid jets issuing from an injector having L/D in the range of 0 to 40, which is typical of the practical fuel injectors, is hardly known, because most of the studies concern themselves with the fully developed jet ($L/D > 40$). From a review of the work done above, it is clear that significant studies have been undertaken to understand the role played by the injector L/D ratio on jet stability in still air, while a similar study for turbulent liquid jets in crossflow is lacking.

The present study extends the recent studies of breakup of liquid jets in gaseous crossflow by Lee et al. [24], Wu et al. [17], Vich and Ledoux [26], Mazallon et al. [27], and Sallam et al. [28] to investigate the effects of the nozzle length/diameter L/D ratio and the nozzle inlet curvature R/D ratio on the breakup characteristics of turbulent liquid jets in gaseous crossflow. The objectives of the present study were to complete new measurements for the onset of drop and ligament formation on the upwind surface, the breakup-regime transitions, and the end of liquid core. The present experiments were carried out using $L/D = 10, 20$, and 40 and $R/D = 0.6, 1.2$, and 2.4.

II. Experimental Methods

A. Apparatus

The experimental setup consisted of the liquid injection system, the crossflow generation and the optical setup. A sketch of the liquid injection system is shown in Fig. 5. The liquid-storage chamber was constructed of type 304 stainless steel and had an inside diameter and length of 76 and 165 mm, respectively. The turbulent round liquid jets were injected vertically downward from a nozzle with a smooth rounded entrance, with different radii of curvature followed by round constant-area passages, as shown in Fig. 6 using an air pressure feed system into the test section of a subsonic wind tunnel. The liquid-jet

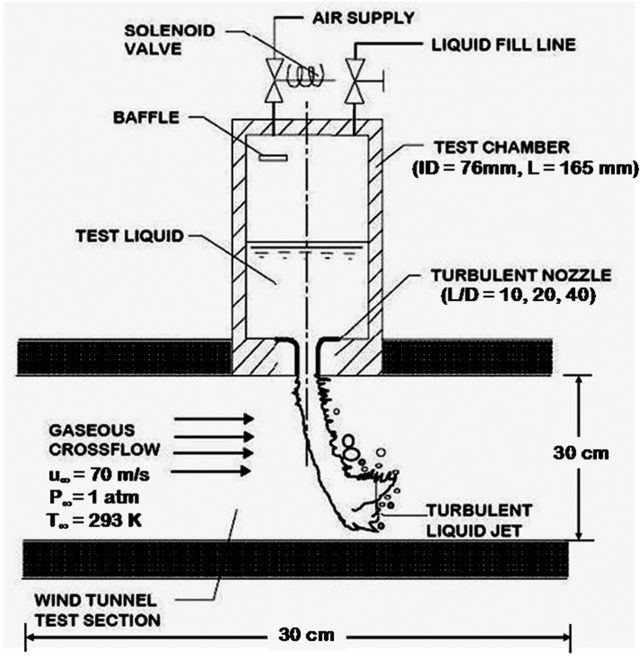

Fig. 5 Sketch of the jet in crossflow apparatus.

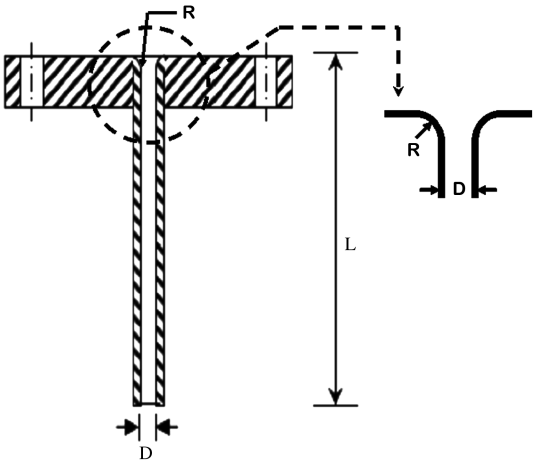

Fig. 6 Sketch of the nozzle geometry used in the present investigation.

injection was initiated by admitting pressurized air to the top of the test chamber by triggering a solenoid valve. The pressurized air was stored on the upstream side of the solenoid valve in an accumulator tank (volume of 0.18 m^3) that was fed with compressed air from a Rix Sweet Air air compressor. The mixing between the air and the test liquid was minimized by a baffle. The liquid injection times were kept long enough such that flow development times and premature outflow did not present problems.

The test section of the open-circuit wind tunnel was made of float glass side walls and floor and an acrylic ceiling to provide optical access. The wind tunnel had a contraction ratio of 16:1, and the velocity variation inside the test section was less than $\pm 1\%$ of mean freestream velocity. The test section was $0.3 \times 0.3 \times 0.6$ m, with air velocities maintained at 70 m/s at normal temperature and pressure, which was measured by a pitot-static tube (United Sensors model PDC-18-G-16-KL) installed at the end of the test section. The pitot-static tube was connected to an inclined tube manometer (Dwyer model no. 400-10-Kit).

B. Instrumentation and Optical Setup

Double-pulsed shadowgraphy and holography microscopy were the two visualization techniques employed. The optics were mounted on a breadboard under the test section of the wind tunnel. The breadboard could be moved horizontally with a resolution of 0.5 mm. The light sources for shadowgraphy and holography were two frequency-doubled Nd:YAG lasers with 7 ns pulse duration (Spectra Physics, Lab 150-10), which could be fired independently and synchronized appropriately to obtain double-pulsed shadowgraphs/holograms. The shadowgraphs/holograms were recorded using double-exposure charge-coupled-device (CCD) camera (PCO 2000, 2048×2048 pixels) that had an interframe time as small as 400 ns. Shadowgraphy, which is a diagnostic in which the intensity of the shadow formed when coherent light is passed through the phase media is dependent on the variations in the optical density of that transparent media, gave the projected size of the droplets and the jet surface structures formed at the jet periphery, but any overlapping ligament or droplet information was lost due to obscurity by the larger structure. Pulsed shadowgraphs can provide a large field of view that is useful for the investigation of the breakup of the liquid column as a whole.

Holography, which is a technique whereby the interference pattern between a wave field scattered from the object after transmission through it and a coherent background (called the reference wave) are recorded photographically [29], does not have the limitation of the depth of field and can be reconstructed at any distance normal to the 2-D image plane. In the present holographic setup, ligaments and jet surface irregularities as small as 5 μm could be observed. The field of view was 8×8 mm. After the hologram was recorded, it was reconstructed numerically. The average intensity was subtracted during the hologram reconstruction. Since the present CCD sensor is

capable of imaging an area of 64 mm^2, the entire region of interest was obtained by recording it in terms of an 8×8 mm area matrix and then combining the images together according to their location. An average sample size of up to 10 holograms was collected at each location. The displacements of jet surface irregularities and ligaments were measured using double-pulsed holograms, and the jet surface velocities were calculated by dividing these displacements by the pulse separation time. The calculated jet surface velocities were calibrated in terms of the nozzle pressure drop. Experimental uncertainties of average jet velocity within 95% confidence were less than 10% dominated by sampling limitations. The measurements considered in the present experiment included the breakup-regime transitions, conditions required for breakup of the liquid column as a whole, and the jet surface characteristics at the jet upwind surface.

C. Test Conditions

The test conditions are summarized in Table 1. The present study was limited to small Ohnesorge number liquid jets ($Oh < 0.01$) injected in crossflow within the shear breakup regime ($We_\infty > 110$). Water was used as the test liquid and was injected from a nozzle with a smooth rounded entrance with different radii of curvature followed by a round constant-area passages having length-to-diameter ratios L/D of 10, 20, and 40. The nozzle diameters D used were 2.0 and 4.0 mm. The values of the radius of curvature of the nozzle passage entry, normalized by the nozzle diameter, R/D, used were 0.6, 1.2, and 2.4. The passage length L, nozzle diameter D, and radius of curvature R at the entry to the nozzle passage are shown in Fig. 6. The different nozzle geometries considered were $L/D = 10$, $D = 4$ mm, and $R/D = 1.2$; $L/D = 20$, $D = 2$ mm, and $R/D = 2.4$; $L/D = 40$, $D = 4$ mm, and $R/D = 1.2$; and $L/D = 40$, $D = 2$ mm, and $R/D = 0.6$. The jets were injected at a Reynolds numbers greater than 10^4 with a noncavitating smooth entry. Gravity effects were negligible for the present test conditions. For gas turbines [30,31] and ramjet engines [32] the fuel is injected into airflow velocities of 15–1000 m/s. The present test conditions are comparable to a nominal range of Ohnesorge (less than 0.1) and crossflow Weber numbers (100–10^5) in those engines.

III. Results and Discussion

A. Flow Visualization

The shadowgraph of the breakup of turbulent jet in crossflow for the test conditions $We_G = 330$, $d_j = 4$ mm, $u_G = 70$ m/s, and $v_j = 20$ m/s are shown in Fig. 7a for $L/D = 10$ and in Fig. 7b for $L/D = 40$. Both nozzles had $R/D = 1.2$. The crossflow is from left to right and the liquid jet was injected vertically downward. The thin wire shown in the background was mounted on the wind-tunnel window to indicate the vertical direction and serves as a reference for cross-stream displacements. The region of interest was recorded into multiple shadowgraphs that were later pasted together according to their respective downstream positions. A similar approach was adopted for visualization of the jet using holographic microscopy. The patched holographic images of the liquid jets up to 20 jet diameters are shown in Fig. 8a injected from a nozzle with $L/D = 20$ and $D = 2$ mm and shown in Fig. 8b injected from a nozzle with $L/D = 40$ and $D = 2$ mm. The field of view of each individual hologram was 8×8 mm. The obtained images revealed a number of general features that were observed during earlier investigations, such as the roughening of liquid surface due to ligament protrusion and surface wave irregularities, relatively close to the jet exit. Subsequently, the size of the liquid-surface roughness elements progressively increased with increasing distance from the jet exit. The small-scale disturbances existed independently of the larger liquid structures appearing far downstream [15,17,33,34]. Small turbulent disturbances appear first and grow faster than large disturbances. The adjustment of turbulent flow after exiting the nozzle passage causes the mean position of the liquid surface to bulge outward near the jet exit. Of interest are the ligaments' formation at the upwind surface, which is a phenomenon that was not observed for the breakup of laminar jets in crossflow [25].

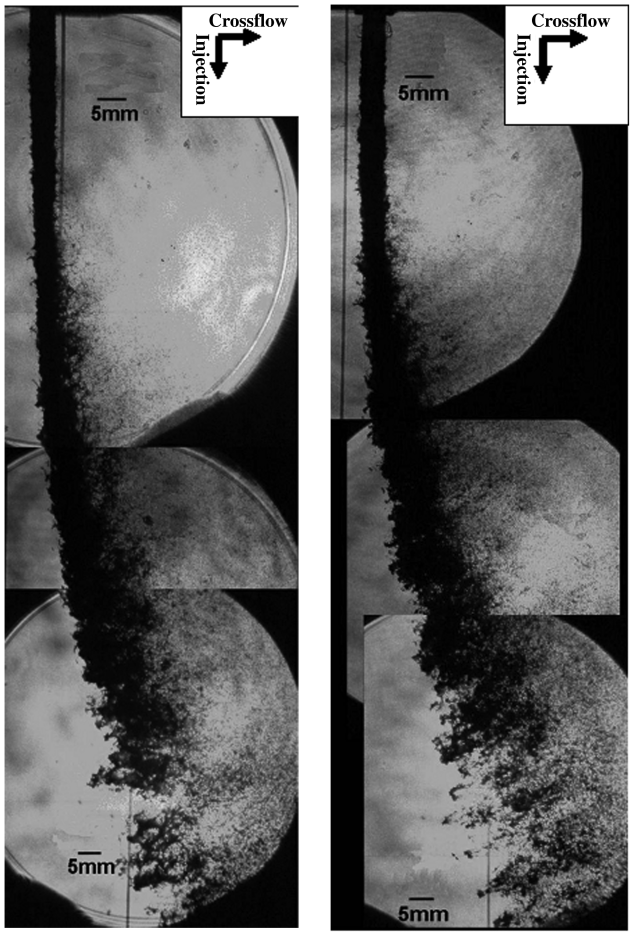

a) b)

Fig. 7 Shadowgraph of turbulent jet in crossflow at a) $L/D = 10$ and $D = 4$ mm at $We_g = 330$, $u_\infty = 70$ m/s, and $v_j = 20$ m/s and b) $L/D = 40$ and $D = 4$ mm at $We_g = 330$, $u_\infty = 70$ m/s, and $v_j = 20$ m/s. The pin indicates the vertical direction.

Table 1 Operating and initial conditions

Parameters	Turbulent
Nozzle diameter, m	0.002, 0.004
Nozzle entrance curvatureR/D	0.6, 1.2, 2.4
Nozzle passage lengthL/D	10, 20, 40
Density of gas, air ρ_{air}, kg/m^3	1.215
Dynamic viscosity of gas, air μ_{air}	1.85E − 05
Surface tension of test liquid, water σ_w, N/m	0.0708
Density of test liquid, water ρ_w, kg/m^3	997
Dynamic viscosity of test liquid μ_w, Ns/m^2	8.94E − 04
Crossflow velocity U_∞, m/s	69
Crossflow Weber number We_∞	376, 332, 166
Jet Weber number We_{LD}	10^4–10^5
Jet velocity V_j, m/s	10–46
Crossflow Reynolds number Re_∞	$\sim 10^4$
Jet Reynolds number Re_{LD}	20000–200000
Ohnesorge number Oh	0.001682

B. Jet Surface Velocities

The streamwise mean liquid-surface velocities for the four nozzles are shown in Fig. 9. Jet surface velocities were calibrated in terms of the nozzle pressure drop by measuring the displacement of jet surface irregularities such as surface waves and ligaments using double-pulsed holograms. The average of the displacements of the jet surface irregularities divided by the delay between the two pulses gave the mean streamwise velocity at that particular streamwise position. Because of the wall retardation effect, the jet surface velocities were

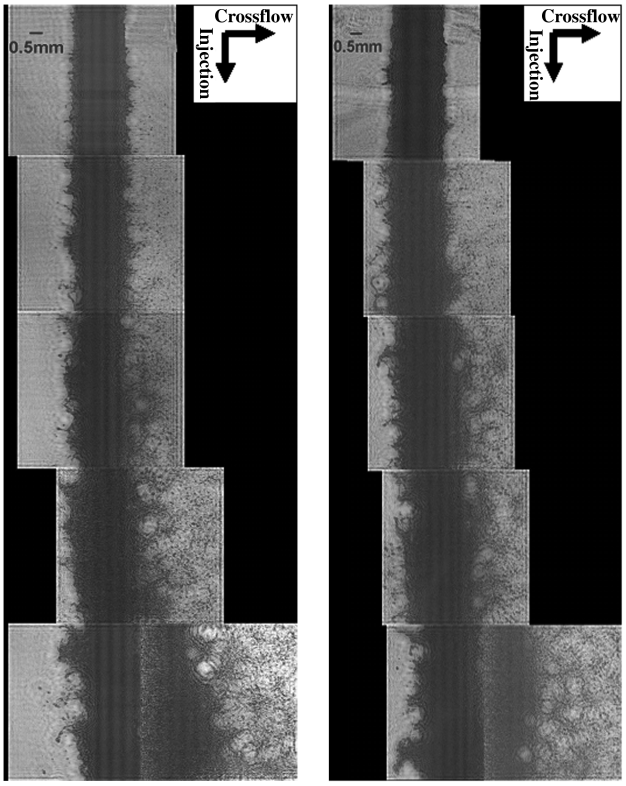

a) b)

Fig. 8 Hologram of the turbulent jet in crossflow for nozzle diameter of 2 mm and a) $L/D = 20$ and b) $L/D = 40$ shown for a distance of 20 jet diameters for $We_g = 170$ and $u_\infty = 70$ m/s.

reduced near the jet exit but increased further away from the nozzle and reached a constant value that was within 10% of the mean value at 15 jet diameters for the present test conditions.

C. Breakup-Regime Transitions

To investigate the breakup-regime transitions, an average sample size of up to 10 holograms constituted a single location. The jet issuing from the longer passage had a greater degree of instability marked by the higher density of surface irregularities and so was more susceptible to earlier breakup. At the upwind surface it had larger and visibly more ligaments showing up, compared to the lower-L/D-ratio jet. At high Reynolds numbers the jet had sufficient turbulent kinetic energy to cause the eddies formed inside the jet to shoot out as ligaments against the upcoming crossflow and form droplets. Depending upon the presence of droplets along the upstream surface, the breakup was classified as turbulent breakup, whereas in the absence of them, the breakup was considered as aerodynamic breakup.

A quantity representing the turbulent–aerodynamic force balance, $We_{L\Lambda}^{m} q^{1/n}$, was phenomenologically derived in order to predict the nature of breakup. The streamwise integral length scale Λ was taken to be $\Lambda = d_j/8$ based on the measurements of Laufer [35] for fully developed turbulent pipe flow, as cited by Hinze [36]. A simplified representation of the ligament-drop formation is shown in Fig. 10. The characteristic size of the eddy causing the onset of ligament formation on the upwind surface is λ, similar to that in [15] in turbulent breakup. The amount of kinetic energy per unit mass in the large-scale turbulence is assumed to be proportional to u^2, where u is the characteristic velocity of the eddies. The transfer rate of energy is proportional to u/l, where l represents the size of the largest eddies and is related to the integral scales of the turbulence. The rate of energy supply to the small-scale eddies is thus on the order of

$$u^2.u/l = u^3/l \tag{1}$$

Correlating the velocity and length scales of the ligament and the largest eddies Λ inside the jet yields

$$(v_{\text{lig}}/v_j)^3 \sim \lambda/\Lambda \tag{2}$$

The turbulent forces within the jet are aiding the formation and growth of ligaments at the upwind surface of the liquid jet, whereas the aerodynamic forces and the surface tension forces are opposing the formation of ligaments at this location. Neglecting the viscous and other dissipative forces associated with the ligament formation process, the energy balance on the upwind surface can be simplified as follows (where KE is kinetic energy):

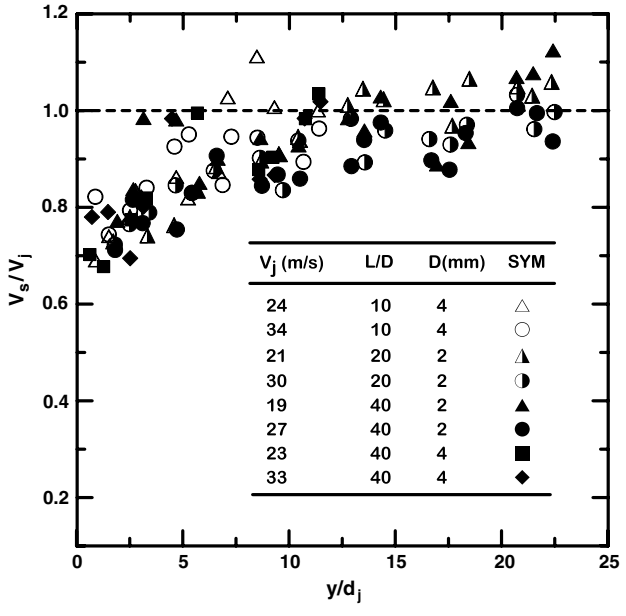

Fig. 9 Mean liquid-surface velocities in the streamwise direction as function of streamwise distance from jet exit.

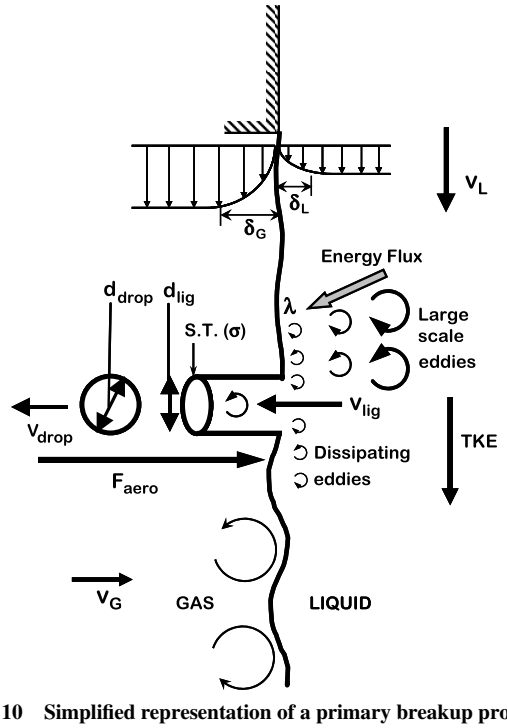

Fig. 10 Simplified representation of a primary breakup process.

$$(\text{turbulent KE})_{\text{lig}} = (\text{aerodynamic work})_{\text{lig}} + (\text{surface tension work})_{\text{lig}} \tag{3}$$

or

$$\rho_L v_{\text{lig}}^2 \lambda^3 \approx C_d \rho_G v_G^2 \lambda^3 + \sigma \lambda^2 \tag{4}$$

or

$$\rho_L v_{\text{lig}}^2 \lambda/\sigma \approx C_d \rho_G v_G^2 \lambda/\sigma + 1 \tag{5}$$

or

$$(\rho_L v_j^2 \Lambda/\sigma)(\lambda/\Lambda)(v_{\text{lig}}/v_j)^2 \approx (C_d \rho_G v_G^2 d_j/\sigma)(\lambda/\Lambda) + 1 \tag{6}$$

or

$$(We_{L\Lambda})(\lambda/\Lambda)(v_{\text{lig}}/v_j)^2 \approx C_d We_G(\lambda/\Lambda) + 1 \tag{7}$$

Substituting λ/Λ from Eq. (2),

$$(We_{L\Lambda})(v_{\text{lig}}/v_j)^5 = C_d We_G(v_{\text{lig}}/v_j)^3 + 1 \tag{8}$$

The above equation could be rewritten in the form of an energy function $E(X)$, where $X = v_{\text{lig}}/v_j$ is the variable parameter affecting the upwind ligament breakup. Of concern here are the minima of $E(X)$ in the neighborhood of zero, since $E(X) > 0$ for the breakup to occur:

$$E(X) = AX^5 + BX^3 + C \tag{9}$$

where $A = We_{L\Lambda}$, $B = -C_d We_G$, and $C = -1$. Setting $\partial E/\partial X = 0$ for minima yields

$$\partial E/\partial X = 5AX^4 + 3BX^2 = 0 \tag{10}$$

or simply

$$X = (v_{\text{lig}}/v_j) = \sqrt{(3C_d We_G)}/\sqrt{(5We_{L\Lambda})} = Z/\sqrt{q}$$

where Z is a constant and $q = We_{L\Lambda}/We_G$. From the present study (see Sec. III.D), Wu and Faeth [16] and Sallam et al. [37], the distance of onset of breakup (Xd_{iu}) can be written as

$$Xd_{iu}/\Lambda \approx K(We_{L\Lambda})^{-m} \tag{11}$$

where K, and m are positive real numbers. The time of onset of breakup is given by Xd_{iu}/v_j. A ligament with velocity v_{lig} should attain its maximum breakup size (i.e. pinch-off length), $L_{\text{pinch off}}$, in the same time. The pinch-off length is then given by $(Xd_{iu}/v_j)v_{\text{lig}}$, or simply

$$L_{\text{pinch off}} = (Xd_{iu})(v_{\text{lig}}/v_j) = K(We_{L\Lambda})^{-m} \cdot (Z/\sqrt{q}) \cdot \Lambda \tag{12}$$

or

$$L_{\text{pinch off}}/\Lambda = K_0/(We_{L\Lambda}^m q^{1/2}) \sim 1 \tag{13}$$

where K_0 is a constant. Generalizing the form above, $We_{L\Lambda}^m q^{1/n}$ represents the nondimensional threshold length of disintegration of the ligaments on the upwind side and should be approximately the same for different nozzles.

To estimate the values of m and n, the breakup map was plotted with $We_{L\Lambda}^m q^{1/n}$ on the y axis vs the crossflow Weber number We_G on the x axis for different values of m and n. The plot of the breakup-regime transition points for $We_{L\Lambda} = 10^3$–10^4; $n = 2$, 3, and 5; and $m = 1$ is shown in Fig. 11. For $n = 3$ the fit through the breakup-regime transition points gives a straight line, thus separating the breakup-regime map into an upper turbulent breakup region and a lower nonturbulent (or aerodynamic) breakup region. The lower aerodynamic region also includes the column, bag, and multimode breakup regimes [37], in addition to the present shear breakup regime. The fit line had a value of $We_{L\Lambda} q^{1/3} \approx 17,000$. In Fig. 12 the plot of $(We_{L\Lambda})^m q^{1/3}$ against the crossflow Weber number We_G for $m = 0$, 1, and 2 is shown. The value of $m = 1$ gives a straight-line fit,

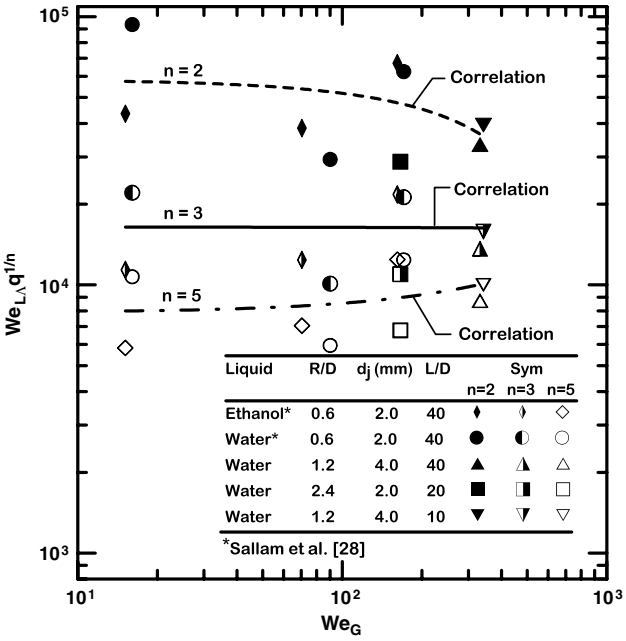

Fig. 11 Jet breakup-regime map of $We_{L\Lambda}q^{1/n}$ vs We_G.

as in the previous case. Though $m = 2$ appears to be a straight-line fit too, it is not so upon closer observation. There is also a larger scatter of the transition points. Thus, the value of $We_{L\Lambda}q^{1/3} = 17,000$ represents the boundary between the turbulent/aerodynamic breakup regimes and is valid within the present experimental uncertainties.

D. Onset of Breakup at the Upwind Surface

The streamwise location of the onset of ligaments (turbulent primary breakup on the upwind surface), $X\text{lig}_{iu}$, and the onset of drop formation, Xd_{iu}, were measured and are plotted against the jet Weber number in Fig. 13. Though the fit follows the same trend of round turbulent liquid jets in still gases for $L/D = 40$ [16,37], the onset of drop formation was observed to occur later. This can be explained by

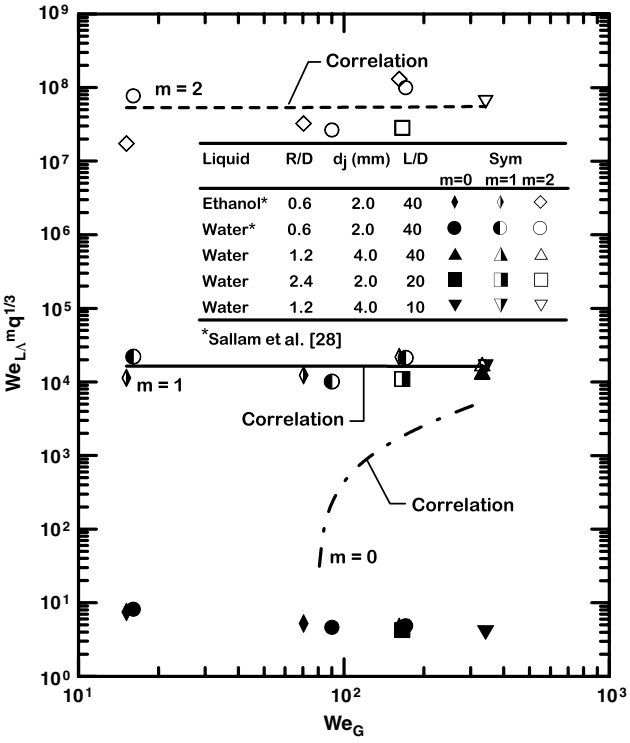

Fig. 12 Jet breakup-regime map of $(We_{L\Lambda})^m q^{1/3}$ vs We_G.

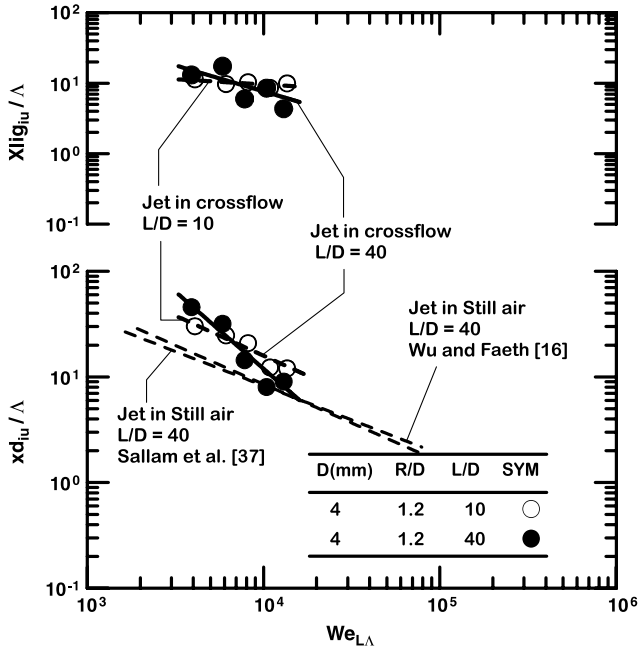

Fig. 13 Onset of breakup against the jet Weber number.

considering the disturbances induced by the aerodynamic forces and the turbulent forces within the jet. On the upwind side the aerodynamic and surface tension forces compete with the dynamic pressure induced by the turbulent eddies within the jet. The onset distance was smaller for the shorter-passage-length nozzle for values of $We_{L\Lambda}$ less than 8000, as compared to its behavior at higher $We_{L\Lambda}$. The observation could be theorized in the following way: the onset of ligaments and drops are brought about by the instabilities in the free liquid surface, which could be due to a number of factors and is usually characterized by the jet Weber number and the nozzle geometry. After leaving the nozzle the shear layer in the jet thins rapidly and the boundary layer relaxes to a free-surface condition from the no-slip condition within the nozzle. Turbulence plays a dominant role in the growth of nonaxisymmetric disturbances and is characterized by eddy vortices that are transformed or propagated radially outward, interacting with the boundary layer and inducing motion/instability of the jet surface. Upon injection, the turbulent eddies start inducing a rollup motion that takes some time and distance to develop, known as the relaxation time t_r and relaxation length l_r, which can be scaled with the nozzle length, respectively [38,39]. At low jet Weber numbers the energy content of the eddies is small. For the shorter-passage nozzle the velocity profile is undeveloped, liquid turbulence is less, and the relaxation length is small in comparison with the longer-passage nozzle, where the turbulence content is relatively high. Also for the shorter nozzle, the velocity relaxation time is less than that of the longer nozzle. Therefore, in the case of the shorter nozzle, the eddies traveling radially outward arrive at the jet surface earlier and with a higher energy to form ligaments and drops earlier than the case of the longer nozzle. However, at higher jet Weber numbers, though the relaxation length and time increase, the exceedingly dominating turbulence in the jet core of the longer-passage nozzle results in the eddies arriving at the jet surface earlier, breaking the relaxation-length barrier, due to their relatively high energy content, thus resulting in quicker surface breakup, as compared to the shorter-passage nozzle. The larger wave instabilities associated with the higher L/D nozzle lead to significantly more atomization and erosion of the liquid core. This phenomenon merits further studies, however.

The correlations of the present measurements (Fig. 13) of the onset of ligaments $X\text{lig}_{iu}$ were as follows:

$$X\text{lig}_{iu}/\Lambda = 6816(We_{L\Lambda})^{-0.74} \quad \text{for } L/D = 40, \qquad D = 4 \text{ mm} \tag{14}$$

$$X\text{lig}_{iu}/\Lambda = 37(We_{L\Lambda})^{-0.15} \quad \text{for } L/D = 10, \qquad D = 4 \text{ mm} \tag{15}$$

The present measurements of the onset of drop formation Xd_{iu} are shown in Fig. 13, together with the experimental correlations for the onset of breakup of liquid jets in still air from [16,37]. The present correlations were

$$Xd_{iu}/\Lambda = 8,258,409(We_{L\Lambda})^{-1.5} \quad \text{for } L/D = 40, \qquad D = 4 \text{ mm} \tag{16}$$

$$Xd_{iu}/\Lambda = 17,244(We_{L\Lambda})^{-0.76} \quad \text{for } L/D = 10, \qquad D = 4 \text{ mm} \tag{17}$$

The correlation coefficient of the fit was 0.97 and 0.96, respectively.

E. Ligament Sizes Along the Upwind Surface of Liquid Jet

The variation of the ligament diameter on the upwind surface as a function of the distance from the jet exit was measured as done by Sallam and Faeth [40] for round free jets. To isolate the L/D effect on the ligament formation characteristics nozzles with the same R/D ratio of 1.2 ($D = 4$ mm) but different L/D ratios (10 and 40) have been considered for the jet Weber number range of $We_{L\Lambda} \sim 3\times 10^4$–$1 \times 10^5$. The present measurements of the ligament diameter normalized by the integral length scale d_{lig}/Λ were plotted vs $y_{\text{lig}}/\Lambda We_{L\Lambda}^{1/2}$ are plotted for $L/D = 10$ and 40 and $R/D = 1.2$ in Fig. 14. The correlations from [40] for $R/D = 1$ and $L/D = 40$ and from [24] for $L/D > 100$ are also shown in Fig. 14. The ligament effective diameter d_{lig} is calculated from the measured ligament length L_{lig} and the ligament projected area on the hologram, A_{lig}, as done in [40] as

$$d_{\text{lig}} = A_{\text{lig}}/L_{\text{lig}} \tag{18}$$

The effective diameter is an approximate representation of the ligament size. It can be seen from Fig. 14 that the ligament size increases along the streamwise direction for both nozzles; the longer L/D nozzle produces larger-sized ligaments. The correlations for the present measurements were as follows:

$$d_{\text{lig}}/\Lambda = 0.40(y_{\text{lig}}/\Lambda We_{L\Lambda}^{1/2})^{0.59} \quad \text{for } R/D = 1.2, \qquad L/D = 40 \tag{19}$$

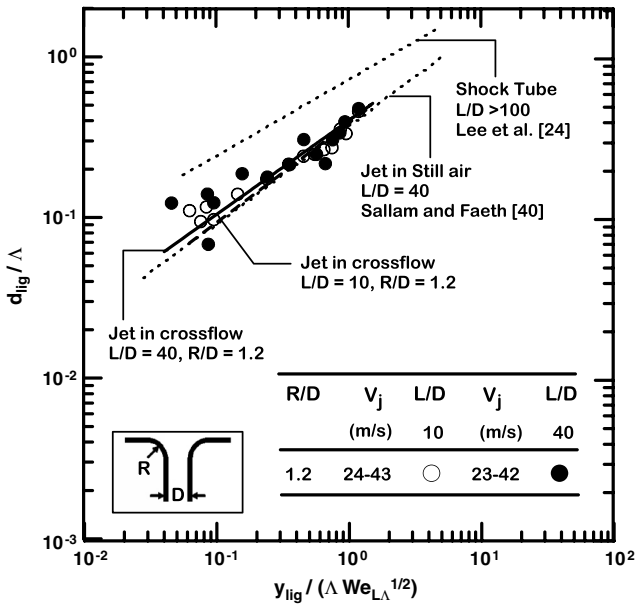

Fig. 14 Ligament size vs the streamwise distance on the upwind surface for different passage lengths and $D = 4$ mm.

$$d_{\text{lig}}/\Lambda = 0.39(y_{\text{lig}}/\Lambda We_{L\Lambda}^{1/2})^{0.62} \quad \text{for } R/D = 1.2, \qquad L/D = 10 \tag{20}$$

The correlation coefficients of the fit were 0.80 and 0.70, respectively. Changing the value of Λ causes the correlations to be displaced along their respective line of slopes, such that a decrease in Λ would result in a displacement away from the origin and an increase in Λ would result in a displacement toward the origin. Next, the measurements were carried out for nozzles with the same L/D ratio of 40, but with R/D ratios of 0.6 and 1.2 and a Weber number range of $We_{L\Lambda} \sim 1 \times 10^4$–$3 \times 10^4$, as shown in Fig. 15. It was observed that the change in the entrance curvature, R/D, causes the correlation of the ligaments size distribution to deviate from the previous correlation to the following:

$$d_{\text{lig}}/\Lambda = 0.47(y_{\text{lig}}/\Lambda We_{L\Lambda}^{1/2})^{0.29} \quad \text{for } R/D = 0.6, \qquad L/D = 40 \tag{21}$$

The correlation coefficient of the fit was 0.73. This could possibly be due to the smaller radii of curvature and it needs a further investigation. The ligament size distribution measurements for nozzles with the same diameter $D = 2$ mm but different L/D (20 and 40) and R/D ratios (2.4 and 0.6) and jet Weber number, $We_{L\Lambda}$, range of 1.3×10^4–4.4×10^4 are shown in Fig. 16. The correlation is given by

$$d_{\text{lig}}/\Lambda = 0.36(y_{\text{lig}}/\Lambda We_{L\Lambda}^{1/2})^{0.37} \quad \text{for } R/D = 2.4, \qquad L/D = 20 \tag{22}$$

Thus, for the same jet diameter the slope of the correlations were closer to each other. The correlation coefficient of the fit was 0.90. It can be observed that with diminishing diameter the ligament size distribution somewhat flattens out. This could be explained by considering the effect of the jet Reynolds number on the onset of primary breakup for turbulent round liquid jets in gaseous crossflow.

A modified form of d_{lig}/Λ, that is $C_1(d_{\text{lig}}/\Lambda)C_2$ was plotted against $(y_{\text{lig}}/\Lambda We_{L\Lambda}^{1/2})$ in Fig. 17 so that the data points fall along the line $R/D = 1$ [40], where C_1 and C_2 would be linear functions of L/D and R/D. Using a fitting routine the coefficients were

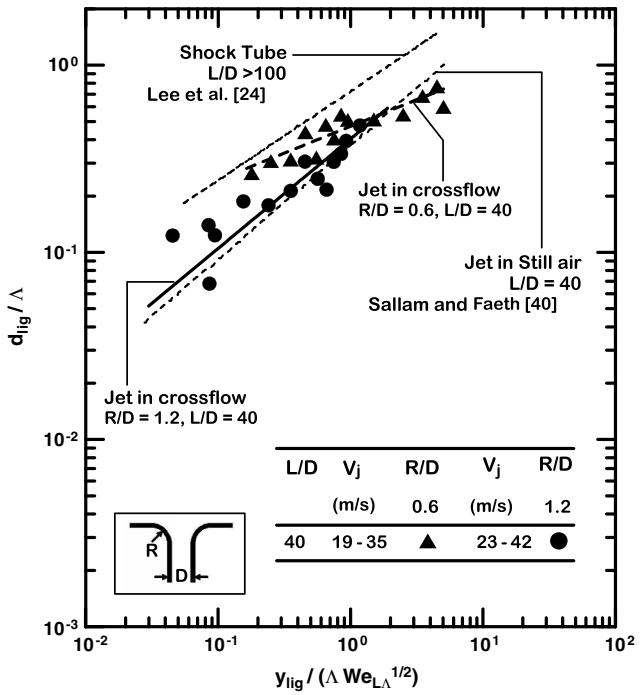

Fig. 15 Ligament size vs the streamwise distance on the upwind surface for nozzles with $L/D = 40$, $D = 4$ mm, and $R/D = 1.2$, and with $L/D = 40$, $D = 2$ mm, and $R/D = 0.6$.

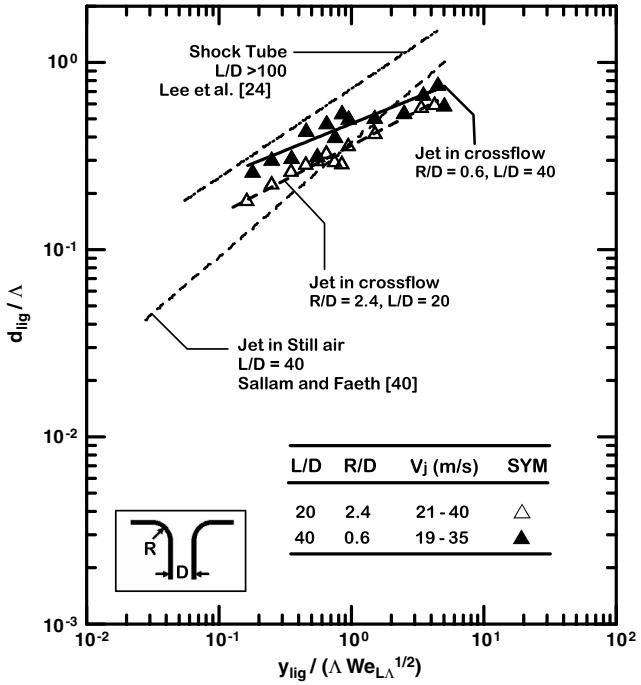

Fig. 16 Ligament size vs the streamwise distance on the upwind surface for $D = 2$ mm nozzles but different passage lengths.

calculated as tabulated in Table 2 and were of the form $a + b(R/D) + c(L/D) + d(L/D)(R/D)$ as following

$$C_1 = -2.59 + 3.19(R/D) + 0.14(L/D) - 0.12(L/D)(R/D) \tag{23}$$

$$C_2 = -2.63 + 3.16(R/D) + 0.16(L/D) - 0.13(L/D)(R/D) \tag{24}$$

Rewriting the above we have

$$d_{\text{lig}}/\Lambda \sim (1/C_1)(y_{\text{lig}}/\Lambda We_{L\Lambda}^{1/2})^{1/C_2} \tag{25}$$

The plot of the modified variables is shown in Fig. 17. In Eq. (25) the crossflow Weber number was kept at a constant value of $u_G = 70$ m/s and only the jet Weber number was varied. Hence, the effect

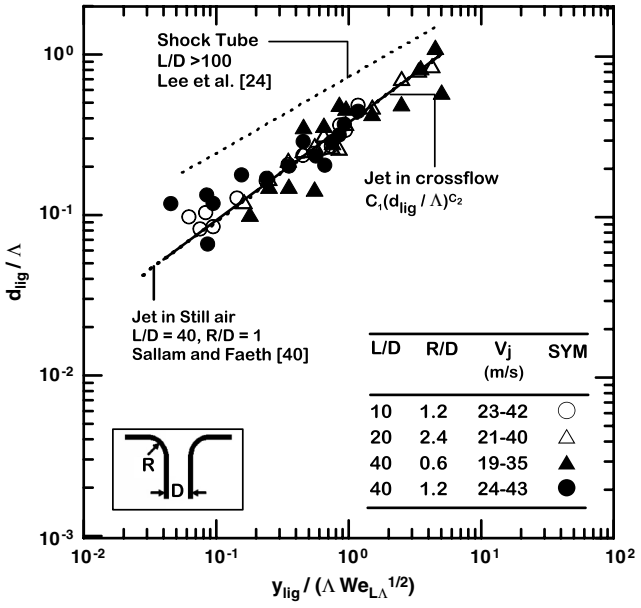

Fig. 17 Modified ligament size vs the streamwise distance on the upwind surface for the different radii of curvature and passage lengths.

Table 2 Coefficients in the $C_1(d_{\text{lig}}/\Lambda)C_2$ vs $(y_{\text{lig}}/\Lambda We_{L\Lambda}^{1/2})$ plot

L/D	R/D	C_1	C_2
10	1.2	1.15	1.12
20	2.4	2.00	1.65
40	1.2	0.91	0.98
40	0.6	1.90	2.30

Table 3 Coefficients in the breakup equation

L/D	n	C_{yb}
4	0.53	3.07
10	0.50	3.29
20	0.50	3.09
40	0.50	2.65

of the aerodynamic forces was not considered. The equation obtained for the final fit line was

$$d_{\text{lig}}/\Lambda = 0.38(y_{\text{lig}}/\Lambda We_{L\Lambda}^{1/2})^{0.61} \tag{26}$$

with a correlation coefficient of the fit equal to 0.78.

F. Breakup of Liquid Core

The breakup downstream distance y_b, the breakup time t_b, and the breakup cross-stream distance x_b were measured from the large-field-of-view shadowgraphs and compared with the data of [17,21,22,25] for $L/D = 0$ (their nozzles are shown in Fig. 4.). It would be helpful to define a turbulent length scale in the context of the nozzle passage length, here. Although the Reynolds numbers of these jets are high the jets issuing from a nozzle with $L/D = 0$ cannot be considered as a turbulent jet, since a certain minimum length in the nozzle is needed before the turbulence (mean flow and fluctuations) becomes developed. Otherwise, it would just be a developing turbulent flow with the turbulent characteristics changing until the flow becomes fully developed. The breakup time t_b of the liquid core, given by

$$t_b = y_b/v_j \tag{27}$$

was analyzed by associating the time of penetration of the jet elements with the aerodynamic characteristic time t^*, given by [41] as

$$t^* = (\rho_L/\rho_G)^{1/2} d_j/u_G \tag{28}$$

The value of t_b/t^* yields the empirical time constant C_{yb} associated with the breakup of the liquid column and its values for different L/D ratios are presented in Table 3, where n is the index of q in the plot (Fig. 19) and is derived from

$$y_b/d_j q = (x_b/d_j q)^n \tag{29}$$

The breakup cross-stream distance, x_b/d_j, has a constant value for a particular L/D as seen in Fig. 18. The measurements of t_b and x_b were plotted as a function of crossflow Weber number together with previous results [24,25] for $L/D = 0$ and were close to the results for nonturbulent jet breakup in gaseous crossflows. The difference in the values of C_{yb} is possibly because the tests for [24,25] were carried out in shock tube with a thinner boundary layer as compared to the boundary layer in a wind tunnel.

The penetration of liquid jets injected into crossflow was also considered in the form similar to that in [25]. The plot of the normalized breakup length, y_b/d_j, as a function of the momentum flux ratio, q, for the three nozzles is shown in Fig. 19. For a complete comparison the present results for $L/D = 10$, 20, and 40 are plotted alongside those of [17,21,22,25]. The following correlations between the breakup length and L/D were obtained:

$$y_b/d_j = 3.3q^{1/2} \qquad L/D = 10, \qquad D = 4 \text{ mm} \tag{30}$$

$$y_b/d_j = 3.1q^{1/2} \qquad L/D = 20, \qquad D = 2 \text{ mm} \tag{31}$$

$$y_b/d_j = 2.7q^{1/2} \qquad L/D = 40, \qquad D = 4 \text{ mm} \tag{32}$$

The correlation coefficients of the fit were 0.98, 0.92, and 0.92, respectively.

It can be seen clearly that with the increase in the nozzle length, the breakup length decreases. The long passage length introduces high turbulence in the jet at high values of momentum ratio, which increases the instabilities induced in the jet and causes an earlier breakup, resulting in shorter breakup lengths. The discrepancy in the breakup behavior between [25] for $L/D = 0$ and [17,21,22] for $L/D = 4$ may be explained by the fact that the measurement of the breakup location from shadowgraphs is subjective and different authors have different criteria of determining the point of breakup. However, a more plausible explanation is that the $L/D = 4$ results were obtained in a wind tunnel [17,22] and a crossflow chamber reproducing the geometry and the operating conditions of the premixing channel of a lean, premixed, prevaporized (LPP) gas turbine engine [21] (where a large boundary layer exists near the nozzle exit) but the results of [25] were obtained in a shock tube (with a thinner boundary layer). In a shock-tube facility the jet experiences the freestream crossflow as soon as it exits the nozzle, whereas in a wind tunnel it would have to cross the wall boundary layer in order to do so, and this could delay its breakup time. This results in a shorter liquid column. For the present investigation, We_G was kept at a fixed value of 166 and 332 in the shear breakup regime, corresponding to a value of Re_G equal to 9×10^3 and 20×10^3 for the 2 and 4 mm nozzles, respectively. The tests by [21] were carried out for LPP gas turbine conditions with water/kerosene at elevated temperatures

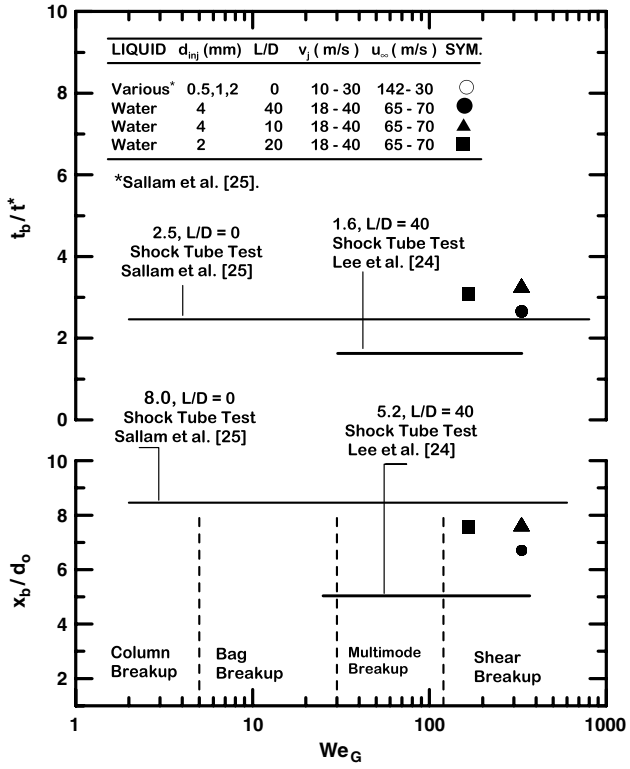

Fig. 18 Plot of jet breakup time and breakup location against the crossflow Weber number.

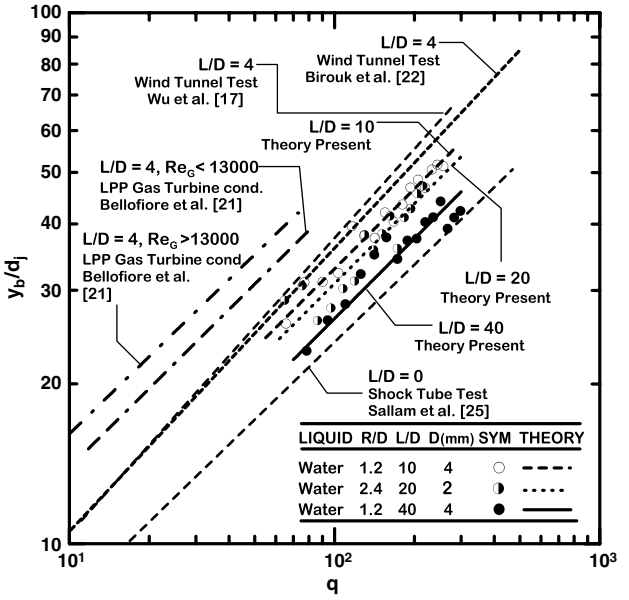

Fig. 19 Breakup length yb/dj as a function of the momentum flux ratio q for $L/D = 10$, 20, and 40.

(300–600 K) and pressures (1–2 MPa) with $Re_G = 5000$ to 26,000 and the breakup length was grouped on the basis of a threshold value of $Re_G = 13,000$.

IV. Conclusions

An experimental study of the effect of the injector geometry on the breakup of turbulent liquid jets in crossflow at STP was conducted. The present investigation involved measurements of the turbulent primary breakup properties at the upwind surface of turbulent round liquid jet in uniform crossflow and the mechanisms involved to find the effects of the nozzle internal geometry. The nozzles used for injecting the liquid jets were designed to have negligible cavitation and had the following geometries: $L/D = 10$, $D = 4$ mm, and $R/D = 1.2$; $L/D = 20$, $D = 2$ mm, and $R/D = 2.4$; $L/D = 40$, $D = 4$ mm, and $R/D = 1.2$; and $L/D = 40$, $D = 2$ mm, and $R/D = 0.6$.

The test conditions included jet exit Reynolds numbers of 20,000–200,000 (corresponding to jet velocities 10–46 m/s), jet exit Weber numbers of 10,000–100,000, and liquid/gas density ratios of 810 at conditions in which direct effects of liquid viscosity were small ($Oh < 0.01$). The major conclusions were as follows:

1) It was observed that the injector passage length does play a role in determining the breakup length and the breakup time. The results show that the increase in the injector L/D ratio resulted in decreasing breakup lengths of turbulent liquid jet for the same jet velocity. It was also observed that the breakup lengths depended on the nature of the crossflow in which the jet was injected. The breakup lengths of turbulent jets in the wind tunnel were different from those observed in the shock tube.

2) The jet upwind-surface characteristics, i.e., onset of ligaments and drops and size of ligaments along the surface, were influenced by the passage length of the injector and the radius of curvature of the nozzle entry. The results were, however, close to turbulent jet in crossflow [24] and turbulent jet in still air [40].

3) The formation of ligaments on the upstream surface of turbulent liquid jet in crossflow was used to classify the breakup-regime map into two major regimes known as aerodynamic breakup regime and turbulent breakup regime. These two regimes are separated by the dimensionless number: $We^m_{L\Lambda} q^{1/n}$.

Finally, measuring turbulence level inside the liquid jet at the nozzle exit is very important to understand the effect of the injector geometry on the turbulent primary breakup mechanism. Measuring the turbulence kinetic energy at the nozzle exit location is needed to provide a better understanding of the role of turbulence in fuel atomization processes.

References

[1] Reitz, R. D., and Braco, F. V., "Mechanism of Atomization of a Liquid Jet," *Physics of Fluids*, Vol. 25, 1982, pp. 1730–1742. doi:10.1063/1.863650

[2] Lin, S., and Reitz, R., "Drop and Spray Formation from a Liquid Jet," *Annual Review of Fluid Mechanics*, Vol. 30, 1998, pp. 105–125. doi:10.1146/annurev.fluid.30.1.85

[3] DeJuhasz, K. J., "Dispersion of Sprays in Solid Injection Oil Engines," *Transactions of the ASME: Oil and Gas Power*, Vol. 53, 1931, pp. 65–74.

[4] Schweitzer, P. H., "Mechanism of Disintegration of Liquid Jets," *Journal of Applied Physics*, Vol. 8, No., 1937, pp. 513–521. doi:10.1063/1.1710333

[5] Bergwerk, W., "Flow Pattern in Diesel Nozzle Spray Holes," *Proceedings of the Institution of Mechanical Engineers*, Vol. 173, 1959, pp. 655–660. doi:10.1243/PIME_PROC_1959_173_054_02

[6] Sadek, R., "Communication on Flow Pattern in Nozzle Spray Holes and Discharge Coefficient of Orifices," *Proceedings of the Institution of Mechanical Engineers*, Vol. 173, No. 25, 1959, pp. 671–672.

[7] Rupe, J. H., "On the Dynamic Characteristics of Free-Liquid Jets and a Partial Correlation with Orifice Geometry," NASA Jet Propulsion Lab., TR 32-207, Pasadena, CA, 1962.

[8] Grant, R. P., and Middleman, S., "Newtonian Jet Stability," *AIChE Journal*, Vol. 12, No. 4, 1966, pp. 669–678. doi:10.1002/aic.690120411

[9] McCarthy, M. J., and Molloy, N. A., "Review of Stability of Liquid Jets and the Influence of Nozzle Design," *Chemical Engineering Journal*, Vol. 7, 1974, pp. 1–21. doi:10.1016/0300-9467(74)80021-3

[10] Sterling, A., and Sleicher, C., "The Instability of Capillary Jets," *Journal of Fluid Mechanics*, Vol. 68, 1975, pp. 477–495. doi:10.1017/S0022112075001772

[11] Hiroyasu, H., Shimizu, M., and Arai, M., "The Breakup of High Speed Jet in a High Pressure Gaseous Atmosphere," *2nd International Conference on Liquid Atomization and Spray Systems (ICLASS)*, 1982, pp. 69–74.

[12] Hiroyasu, H., Arai, M., and Shimizu, M., "Breakup Length of a Liquid Jet and Internal Flow in a Nozzle," *International Conference on Liquid Atomization and Spray Systems*, 1991, pp. 123–133.

[13] Hiroyasu, H., "Spray Breakup Mechanism from the Hole Type Nozzle and its Application," *Atomization and Sprays*, Vol. 10, 2000, pp. 511–527.

[14] Arai, M., Shimizu, M., and Hiroyasu, H., "Breakup Length and Spray Angle of High Speed Jet," *3rd International Conference on Liquid Atomization and Spray Systems*, 1985.

[15] Wu, P.-K., Miranda, R. F., and Faeth, G. M., "Effects of Initial Flow Conditions on Primary Breakup of Nonturbulent and Turbulent Round Liquid Jets," *Atomization and Sprays*, Vol. 5, 1995, pp. 175–196.

[16] Wu, P. K., and Faeth, G. M., "Onset and End of Drop Formation Along the Surface of Turbulent Liquid Jets in Still Gases," *Physics of Fluids*, Vol. 7, 1995, pp. 2915–2917. doi:10.1063/1.868667

[17] Wu, P. K., Kirkendall, A. K., Fuller, P. R., and Nejad, A. S., "Breakup Processes of Liquid Jets in Subsonic Crossflows," *Journal of Propulsion and Power*, Vol. 13, No. 1, 1997, pp. 64–73. doi:10.2514/2.5151

[18] Cavaliere, A., Ragucci, R., and Noviello, C., "Bending and Break-Up of a Liquid Jet in a High Pressure Airflow," *Experimental Thermal and Fluid Science*, Vol. 27, 2003, pp. 449–454. doi:10.1016/S0894-1777(02)00246-7

[19] Yoon, S., "Droplet Distributions at the Liquid Core of a Turbulent Spray," *Physics of Fluids*, Vol. 17, 2005, pp. 1–24. doi:10.1063/1.1852577

[20] Zhang, J., Jiang, D., Huang, Z., Obokata, T., Shiga, S., and Araki, M., "Experimental Study on Flashing Atomization of Methane/Liquid Fuel Binary Mixtures," *Energy and Fuels*, Vol. 19, No. 5, 2005, pp. 2050–2055. doi:10.1021/ef0500742

[21] Bellofiore, A., Cavaliere, A., and Ragucci, R., "Air Density Effect on the Atomization of Liquid Jets in Crossflow," *Combustion Science and Technology*, Vol. 179, No. 1, 2007, pp. 319–342. doi:10.1080/00102200600809563

[22] Birouk, M., Azzopardi, B. J., and Stäbler, T., "Primary Break-Up of a Viscous Liquid Jet in a Cross Airflow," *Particle & Particle Systems*

Characterization, Vol. 20, No. 4, 2003, pp. 283–289.
doi:10.1002/ppsc.200390034
[23] Mashayek, A., and Ashgriz, N., "Model for Deformation of Drops and Liquid Jets in Gaseous Crossflows," *AIAA Journal*, Vol. 47, No. 2, 2009, pp. 303–313.
doi:10.2514/1.36148
[24] Lee, K., Aalburg, C., Diez, F. J., Faeth, G. M., and Sallam, K. A., "Primary Breakup of Turbulent Round Liquid Jets in Uniform Crossflows," *AIAA Journal*, Vol. 45, No. 8, 2007, pp. 1907–1916.
doi:10.2514/1.19397
[25] Sallam, K. A., Aalburg, C., and Faeth, G. M., "Breakup of Round Nonturbulent Liquid Jets in Gaseous Crossflows," *AIAA Journal*, Vol. 42, No. 12, 2004, pp. 2529–2540.
doi:10.2514/1.3749
[26] Vich, G., and Ledoux, M., "Investigation of a Liquid Jet in a Subsonic Cross Flow," *7th International Conference on Liquid Atomization and Spray Systems*, 1997, pp. 23–30.
[27] Mazallon, J., Dai, Z., and Faeth, G. M., "Primary Breakup of Nonturbulent Round Liquid Jets in Gas Crossflows," *Atomization and Sprays*, Vol. 9, No. 3, 1999, pp. 291–311.
[28] Sallam, K. A., Ng, C.-L., Sankarakrishnan, R., Aalburg, C., and Lee, K., "Breakup of Turbulent and Non-Turbulent Liquid Jets in Gaseous Crossflow," AIAA Paper 2006-1517, 2006.
[29] Schnars, U., and Juptner, W., "Digital Recording and Numerical Reconstruction of Holograms," *Measurement Science & Technology*, Vol. 13, 2002, pp. R85–R101.
doi:10.1088/0957-0233/13/9/201
[30] Giampaolo, T., *Gas Turbine Handbook: Principles and Practice*, 3rd ed., Fairmont, Liburn, GA, 2006.
[31] Boyce, M. P., *Gas Turbine Engineering Handbook*, 3rd ed., Elsevier Science, New York, 2006.
[32] Hojnacki, J. T., "Ramjet Engine Fuel Injection Studies," U.S. Air Force Aero Propulsion Lab, TR AFAPL-TR-72-76, Wright-Patterson AFB, OH, Nov. 1972.
[33] Tseng, L.-K., Ruff, G. A., and Faeth, G. M., "Effects of Gas Density on the Structure of Liquid Jets in Still Gases," *AIAA Journal*, Vol. 30, 1992, pp. 1537–1544.
doi:10.2514/3.11098
[34] Ruff, G. A., Sagar, A. D., and Faeth, G. M., "Structure and Mixing Properties of Pressure-Atomized Sprays," *AIAA Journal*, Vol. 27, No. 7, 1989, pp. 901–908.
doi:10.2514/3.10198
[35] Laufer, J., "The Structure of Turbulence in Fully Developed Pipe Flow," NACA Rept. 1174, 1954.
[36] Hinze, J. O., *Turbulence*, 2nd ed., McGraw–Hill, New York, 1975.
[37] Sallam, K. A., Dai, Z., and Faeth, G. M., "Drop Formation at the Surface of Plane Turbulent Liquid Jets in Still Gases," *International Journal of Multiphase Flow*, Vol. 25, 1999, pp. 1161–1180.
doi:10.1016/S0301-9322(99)00042-7
[38] Gordillo, J. M., and Perez-Saborid, M., "Aerodynamic Effects in the Break-Up of Liquid Jets: On the First Wind-Induced Break-Up Regime," *Journal of Fluid Mechanics*, Vol. 541, 2005, pp. 1–20.
doi:10.1017/S0022112005006026
[39] Yoon, S. S., and Heister, S. D., "A Nonlinear Atomization Model Based on a Boundary Layer Instability Mechanism," *Physics of Fluids*, Vol. 16, No. 1, 2004, pp. 47–61.
doi:10.1063/1.1629301
[40] Sallam, K. A., and Faeth, G. M., "Surface Properties during Primary Breakup of Turbulent Liquid Jets in Still Air," *AIAA Journal*, Vol. 41, No. 8, 2003, pp. 1514–1524.
doi:10.2514/2.2102
[41] Ranger, A. A., and Nicholls, J. A., "The Aerodynamic Shattering of Liquid Drops," *AIAA Journal*, Vol. 7, No. 2, 1969, pp. 285–290.
doi:10.2514/3.5087

K. Frendi
Associate Editor